SNAP-THROUGH BUCKLING ANALYSIS OF A SHALLOW GEODESIC DOME USING MSC/NASTRAN

by

S. LOGANATHAN, BSc Eng Civil (Hons),M.Eng, PhD
Senior Structural Engineer
and
R.C. MORGAN, BE, M.Eng Sc, MIE Aust
Principal Consultant - Structural

BHP ENGINEERING, BRISBANE, AUSTRALIA 4000

ABSTRACT

This paper illustrates the nonlinear analytical and experimental study of a shallow geodesic dome comprising thin walled circular hollow sections. A 156-member shallow geodesic dome that has a rise to span ratio of 1:10 (ie. a rise of 0.6m to span of 6.0m) was constructed and tested experimentally. The present investigation is focused to study the snap-through phenomena of the dome subjected to a static load at the centre of the dome. The dome is discretized as 156 beam elements and its perimeter supports are assumed as ideal pin supports. Displacement control of the load point was employed to trace snap-through and this prevents any possible dynamic jump in the vicinity of the snap-through region. Experimental observation shows that the members near the loading point deformed severely under the applied load without resulting in any damage to the welded joints, apart from material yielding in certain members.

MSC/NASTRAN Version 67 installed on the BHP Research CRAY-YMP (EL) SuperComputer was used as the numerical tool to validate the complex nonlinear behaviour of the dome. The results of geometrical and material nonlinear analysis of the dome from MSC/NASTRAN compare well with the experimental results for cases where the displacements can be reasonably measured with the linear transducers employed. A second nonlinear large displacement analysis was carried out with MSC/NASTRAN on a Schwedler dome in which the connection details are based on the Harley Spaceframe structures. The Schwedler dome considered has a rise-to-span ratio of 1:4 (ie., a rise of 2.5 m to span of 10.0 m).

1.0 INTRODUCTION

In general, large displacement analysis of a structural system consisting of many members is very complex due to the nature of the governing differential equations. Nonlinear closed form solutions are not readily available for the differential equations. However, there are some approximate methods available to solve the nonlinear problems. Series solution was one of the earliest approximate methods employed in the geometric nonlinear analysis. Researchers in the past experienced limitations with this method due to the application of complex loading and boundary conditions. To circumvent these problems, numerical methods based on the finite difference method, the finite element method and the boundary element method have been developed. Among those methods, the finite element method was found to be the most powerful technique to study the large displacement behaviour of structures.

Although the finite element method was firmly established and extensively used in the late sixties, the geometric and material nonlinear analysis of spatial structures has received considerable attention over the past decade. This may be partly due to the usage of light weight materials and design, especially in the field of optimal structural designs where the instability phenomenon may become the critical design criterion. As such, the evaluation of post critical structural response has become inevitable. In structural design, the evaluation of accurate ultimate loads of structures is an important task. In order to determine the accurate ultimate load, both nonlinearities originating from material and geometry must be incorporated in the analysis. The material nonlinearity arises due to the nonlinear stress-strain relationship while the geometric nonlinearity is a consequence of the changes of configuration during the loading process. It is therefore of interest to examine their response under limiting loads at which the structural capacity is exhausted.

In describing the motion of the element an updated Lagrangian description [1-3] was employed in the present study. The analysis of geodesic dome structures in the post-buckling range by means of the finite element method inevitably involves the solution of large systems of nonlinear equations. The most satisfactory way of solving such problems is to combine the arc length method (Riks and Crisfield) within each increment with the Newton-Raphson method (NR method) as the iteration strategy.

In practice, light weight dome structures have been preferred by designers to cover large span areas such as sports stadium, exhibition and assembly halls, swimming pools, shopping arcades and industrial buildings since the need of intermediate supports is minimal. The shallow geodesic dome structures subjected to external loads often reveal various types of instability phenomena such as the snap-through buckling and the buckling of the bifurcation type (refer Fig. 2.1).

2.0 USEFUL FEATURES OF MSC/NASTRAN

MSC/NASTRAN nonlinear capabilities are well documented in MSC's Handbook for Nonlinear Analysis [4]. The special features of nonlinear finite element analysis are highlighted in the above document. The success of the nonlinear analysis is heavily dependent on the numerical algorithm employed in obtaining the solution. A collection of nonlinear finite element solution strategies which are incorporated in MSC/NASTRAN (Version 65, 66 and 67) are briefly summarised in Ref. [4]. It appears that most of the existing numerical techniques are not adequate to ensure convergence, stability and efficiency if overall structural response is to be traced. The conventional Newton-Raphson iteration method which employs load control has often failed in the vicinity of critical points.

This method alone is not efficient enough to handle the snap-through problem. Also, it requires an increasing number of iterations when the stiffness matrix approaches singularity and in many instances the final solution may even diverge.

Researchers in the past proposed various numerical strategies to overcome these problems and to trace the load deflection path well beyond the critical point. Some of the numerical methods are (i) the pure incremental method, (ii) the artificial spring method, (iii) the displacement control method, (iv) the constant work method , and (v) the arc length method. The displacement control method in which the iterations are performed at a constant displacement for a particular degree of freedom is robust enough to handle simple snap-through problems. However, it is not sufficiently stable to trace those load deflection curves with snap-back characteristics. The arc length method has been found to be more suitable to trace both snap-through and snap-back phenomena.

The accuracy and overall efficiency of nonlinear finite element analysis solely depends on the selection of the convergence test. In an iterative process, the out-of-balance forces and the changes in displacement should vanish when solution converges to a stable equilibrium. The iterative process is terminated once the convergence test is passed. The convergence test and the related problems are well documented in Ref. [4].

3.0 CRISFIELD'S CONSTANT ARC LENGTH SOLUTION METHOD

The conventional Newton-Raphson method alone is not capable enough to trace the nonlinear response of a dome structure beyond the critical limit point. In general, the post-buckling behaviour of structures are not allowed for in the design process. However, the prediction of post-buckling behaviour of dome structures becomes desirable to trace the snap-through buckling. Even though, the arc length method is not a particularly efficient solution technique, it is an effective solution strategy in the vicinity of limit points.

The constraint equation described in Refs. [5,6] which couples all the displacements and external incremental loads through fixing the length of the increment as depicted in Fig. 3.1, i.e.,

$$\{\Delta u\}^T\{\Delta u\} + \Delta\lambda^2\{\Delta P\}^T\{\Delta P\} = \Delta l^2 \qquad (1)$$

where Δl is the incremental arc-length.

The above constraint equation was originally added with the incremental stiffness matrix. Unfortunately, the inclusion of an additional constraint equation destroys the symmetry and bandedness of the stiffness matrix. The constraint equation was reformulated by Crisfield [7] for the purpose of numerical analysis and its superiority has been numerically proven by many researchers.

The modified constraint equation is as follows:

$$\{\Delta u\}^T\{\Delta u\} = \Delta l^2 . \qquad (2)$$

This implies that the magnitude of the displacement vector is constrained. At the first load increment, a unit loading parameter or load factor (i.e., $\Delta\lambda^{(1)} = 1$) is chosen as the scalar multiplier of an arbitrary external load and the incremental displacement is determined by the following equation:

$$\{\Delta u^{(1)}\} = [k]^{-1}\,\Delta\lambda^{(1)}\{P\}\,. \tag{3}$$

Hence, the prescribed generalised arc length

$$\Delta l = \sqrt{\{\Delta u^{(1)}\}^{T}\{\Delta u^{(1)}\}}\,. \tag{4}$$

The sign of incremental load factor is determined by the sign change of the incremental work done, ΔW, where

$$\Delta W = \{\Delta u^{(1)}\}^{T}\{P\}\,. \tag{5}$$

If the sign of ΔW has changed from that of the previous increment, the sign of $\Delta\lambda^{(1)}$ is reversed from that of its previous value.

At the i-th iteration, after the initial increment,

$$\{\Delta u_e^{(i)}\} = [k]^{-1}\{P\} \tag{6}$$

and

$$\{\Delta u_r^{(i)}\} = [k]^{-1}\{R^{(i-1)}\}\,, \tag{7}$$

where $\{R^{(i-1)}\}$ is the residual force at the end of the (i-1)-th iteration.

The iterative displacement $\{\Delta u^{(i)}\}$ is,

$$\{\Delta u^{(i)}\} = \Delta\lambda^{(i)}\{\Delta u_e^{(i)}\} + \{\Delta u_r^{(i)}\}\,. \tag{8}$$

The incremental displacement up to the i-th iteration $\{\delta u^{(i)}\}$ is given by,

$$\{\delta u^{(i)}\} = \{\delta u^{(i-1)}\} + \{\Delta u^{(i)}\}\,. \tag{9}$$

According to Eqn. (4),

$$\{\delta u^{(i)}\}^{T}\{\delta u^{(i)}\} = \Delta l^{2}\,. \tag{10}$$

Substituting Eqns. (8) and (9) into Eqn. (10) results in,

$$a(\Delta\lambda^{(i)})^2 + b(\Delta\lambda^{(i)}) + c = 0\,, \tag{11}$$

where,

$$a = \{\Delta u_e^{(i)}\}^T\{\Delta u_e^{(i)}\}\,,$$

$$b = 2[\{\delta u^{(i-1)}\} + \{\Delta u_r^{(i)}\}]^T\{\Delta u_e^{(i)}\}\,,$$

$$c = [\{\delta u^{(i-1)}\} + \{\Delta u_r^{(i)}\}]^T[\{\delta u^{(i-1)}\} + \{\Delta u_r^{(i)}\}] - \Delta l^2\,.$$

The real roots are possible if and only if

$$b^2 - 4ac \geq 0\,. \tag{12}$$

Selection of appropriate root was suggested by Crisfield [7] to avoid doubling back on the solution path. This will be such that the angle between the previous incremental displacement $\{\delta u^{(i-1)}\}$ and the present incremental displacement $\{\delta u^{(i)}\}$ should be positive. If both choices of $\Delta\lambda^{(i)}$ result in positive values, then the appropriate root is the one nearest to the linear solution,

$$\Delta\lambda^{(i)} = -c/b\,. \tag{13}$$

4.0 EXAMPLES

4.1 A Shallow Geodesic Dome

A shallow geodesic dome, 1:10 rise-to-span ratio, shown in Fig. 4.1 has been selected to study the snap-through buckling behaviour. In the present analysis, the dome is discretized as 156 beam elements (see Fig. 4.2) and its perimeter supports are assumed as ideal pin supports. Displacement control of the load point was employed to trace snap-through and this prevents any possible dynamic jump in the vicinity of the snap-through region. All the members were welded to form the overall configuration of the dome.

The external load was applied at the centre of the dome (see Fig. 4.2, Node 1) and the displacement was controlled by means of the Instron Mini Controller.

Measurements for nodal displacements and rotations were recorded at selected joints. The analytical and experimental results for vertical displacements at nodes 1, 2 and 14 (see Fig. 4.2) and rotation at node 58 are shown in Figs. 4.3 - 4.7. It appears from Fig. 4.3 that the experimental results are in reasonable agreement with the numerical results from MSC/NASTRAN in the snap-through region. It is interesting to note that the results obtained from MSC/NASTRAN were slightly lower than the experimental results.

The experimental load displacement curve for node 2 (see Fig. 4.4) is not in particularly good agreement with the numerical results. However, the same trends are observed in both the numerical and experimental curves. One should notice that the displacement of the node is relatively small and it is recognized that the accuracy of the linear transducers used to measure the vertical displacements is not good in this range. Similar problems with small displacements are highlighted for node 14 as shown in Fig. 4.5. The support rotation at node 58 (see Fig. 4.2) is depicted in Fig. 4.6. In this case, numerical and experimental results do not correlate well with each other. However, it is interesting to note in each of these plots how the support rotations are correlated with snap-through behaviour of the dome.

A partial listing of the case control and the bulk data of MSC/NASTRAN input data for this example is shown below:

```
SUBCASE 1
      LOAD      =   1
      SPC       =   1
      NLPARM    =   2671
BEGIN BULK
PARAM, K6ROT, 100000.
PARAM, LGDISP, 1
NLPARM, 2671,60,,AUTO,,,PW, YES
NLPCI, 2671,,1.0,1.0,,,20,250
PARAM     POST     0
$
FORCE     1  1      0       3000.                          -1.
$
MAT1      1  199900.         .27      7.85-6   1.17-5
MATS1,1,,PLASTIC,1326.3,,,235.
$
ENDDATA
```

4.2 A Schwedler Dome

The Schwedler dome that has a rise-to-span ratio of 1:4 (i.e., a rise of 2.5 m to span of 10.0 m) is selected to study the post-buckling behaviour and hence to propose an testing program for Harley Systems. The geometry and the plan view of this dome is shown in Figures 4.7 and 4.8, respectively.

In the Finite Element discretization of the dome, all the radial members and first and third ring members are considered as beam elements and the others are considered as rod elements. A static asymmetric load is applied at node 4 to trace the snap-through behaviour using MSC/NASTRAN Version 67 on the BHP Research CRAY-YMP (EL) Supercomputer.

The numerical results from both linear and nonlinear analyses are plotted together for direct comparison. Load displacement curves for nodes 1, 2, 4, 6, 8 and 10 (see Fig. 4.8) are depicted in Figures 4.9 - 4.14, respectively. Also, the support rotations at nodes 12, 18, 28 and 39 are shown in Figures 4.15 - 4.18. Axial loads for selected members are also illustrated in Figures 4.19 - 4.26. It is interesting to note from all these results that how the nonlinear analysis results differ from linear analysis results.

5.0 CONCLUSION

The present work describes the loading characteristics of a shallow geodesic dome and a Schwedler dome manufactured from mild steel circular and square hollow tubes. The nonlinear analytical results of the geodesic dome using MSC/NASTRAN compares well with the experimental results within the snap-through range for nodes at which the displacements can be reasonably measured. Experimental observation of the geodesic dome showed that the members near the loading point deformed severely under the applied load without resulting any damage to the welded joints, apart from material yielding in certain members.

The load displacement characteristics of the Schwedler dome by incorporating both geometric and material nonlinearity is presented. The results of linear analysis of the dome show a considerable difference with the large displacement analysis in which the material nonlinearity is considered. The arc length method available is MSC/NASTRAN Version 67, was found to be an excellent numerical tool to trace the load displacement path of single layer domes which are prone to snap-through buckling.

6.0 ACKNOWLEDGEMENT

The authors wish to acknowledge and thank Mr Andrew Lewis and Andre Joanise of BHP Research Laboratories for their assistance with the CRAY YMP (EL) Supercomputer and to Dr Andrew Currie of Compumod and his colleagues for their invaluable help in using MSC/NASTRAN. The authors would also like to thank BHP Engineering Pty Ltd for providing financial support in the presentation of this paper.

7.0 REFERENCES

[1]. Meek, J.L. and Loganathan, S., "Large Displacement Analysis of Space Frame Structures", Computer Methods in Applied Mechanics and Engineering, Vol. 72, No. 1, 1989, pp. 57-75.

[2]. Meek, J.L. and Loganathan, S., "Theoretical and Experimental Investigation of a Shallow Geodesic Dome of Circular Hollow Steel Tube", International Journal of Space Structures, Vol. 4, No. 2, 1990, pp. 89 - 105.

[3]. Loganathan, S., Geometric and Material Nonlinear Behaviour of Space Frame Structures, Ph.D. Thesis, Dept. of Civil Engineering, University of Queensland, Australia, February 1989.

[4]. Lee, S.H., MSC/NASTRAN - Handbook for Nonlinear Analysis (Based on Version 65/66/67), The MacNeal-Schwendler Corporation, Los Angeles, CA 90041, July 1991.

[5]. Riks, E., "An incremental approach to the solution of snapping and buckling problems", International Journal of Solids and Structures, Vol. 15, 1979, pp. 529 - 551.

[6]. Wempner, G.A., "Discrete approximations related to nonlinear theories of solids", International Journal of Solids and Structures, Vol. 7, 1971, pp. 1581 - 1599.

[7] Crisfield, M.A., "A fast incremental/iterative solution procedure that handles snap-through", Computers & Structures, Vol. 13, 1981, pp. 55 - 62.

[8] Logantahan, S, and Morgan, R C, "Snap-Through Buckling Analysis of a Shallow Reodesci Dome Wing MSC/NASTRAN", The Fifth Australasian MSC Users Conference, Sydney, Australia, Nov. 1991.

(a) Snapping (b) Buckling

Fig. 2.1 Problem Types

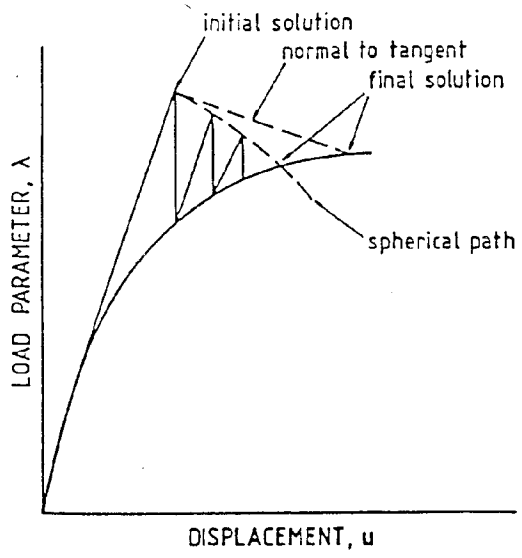

Fig. 3.1 Constraint Surfaces for the Arc Length Method

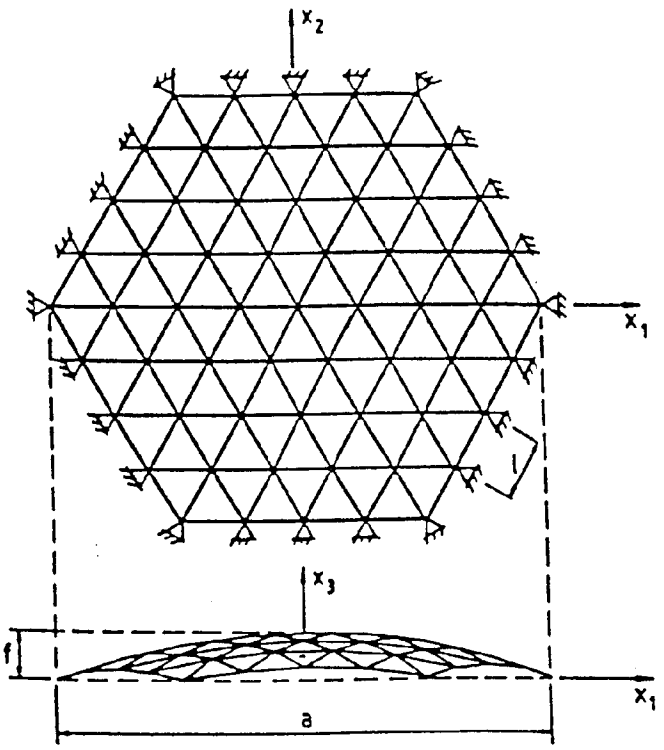

$\nu = 0.3$

E = 220.0 GPa

A = 151.3 mm^2

a = 6.0 m

f = 0.6 m

l = 0.75 m

Equation of surface:

$x_1^2 + x_2^2 + (x_3 + 7.2)^2 = 60.84$

Fig. 4.1 Geometry of the Shallow Geodesic Dome

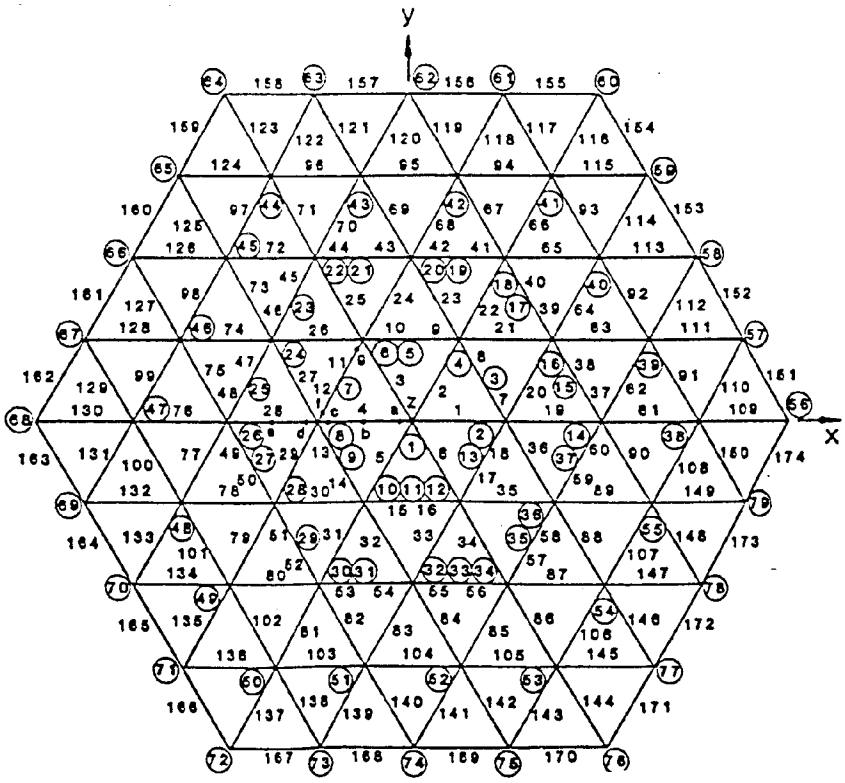

Fig. 4.2 Finite Element Discretisation of the Dome

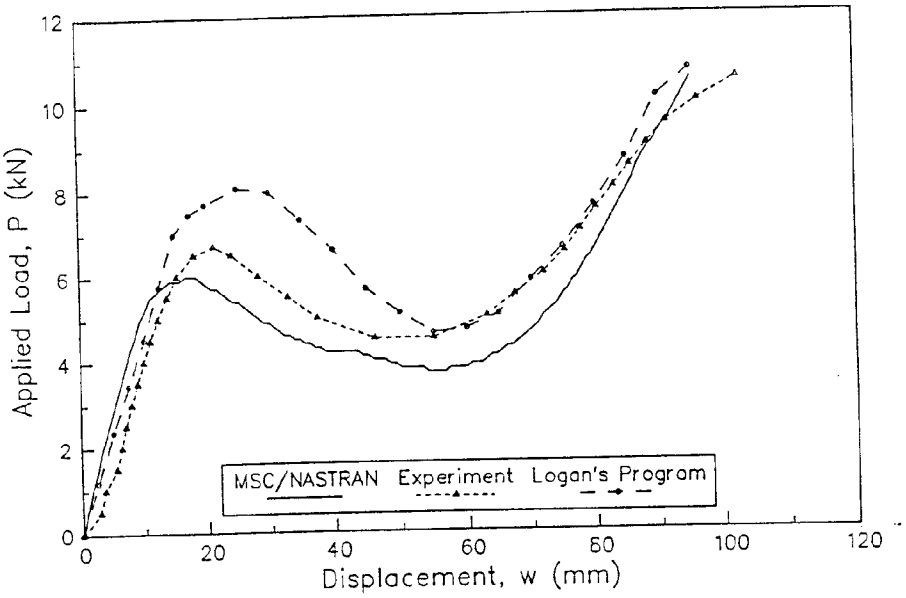

Fig. 4.3 Load Displacement Curve at Node 1

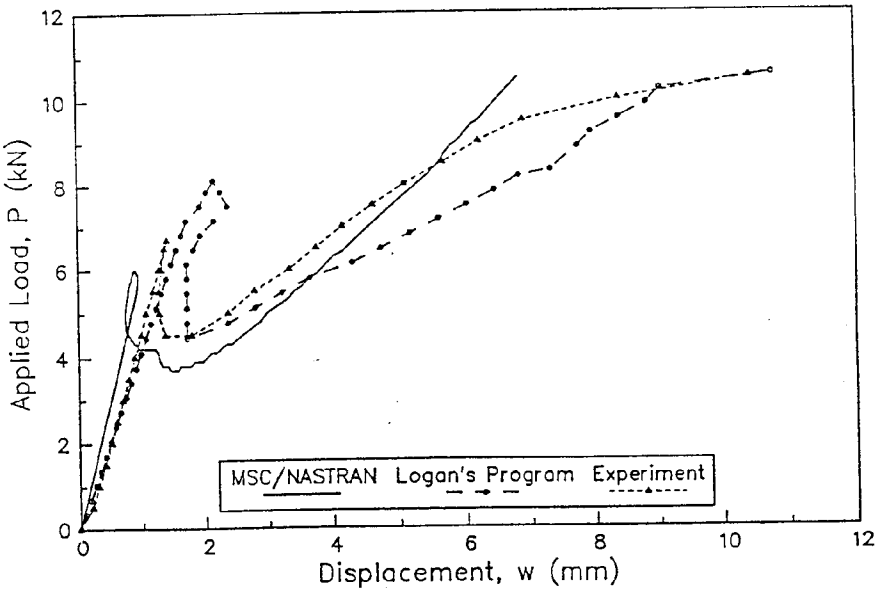

Fig. 4.4 Load Displacement Curve at Node 2

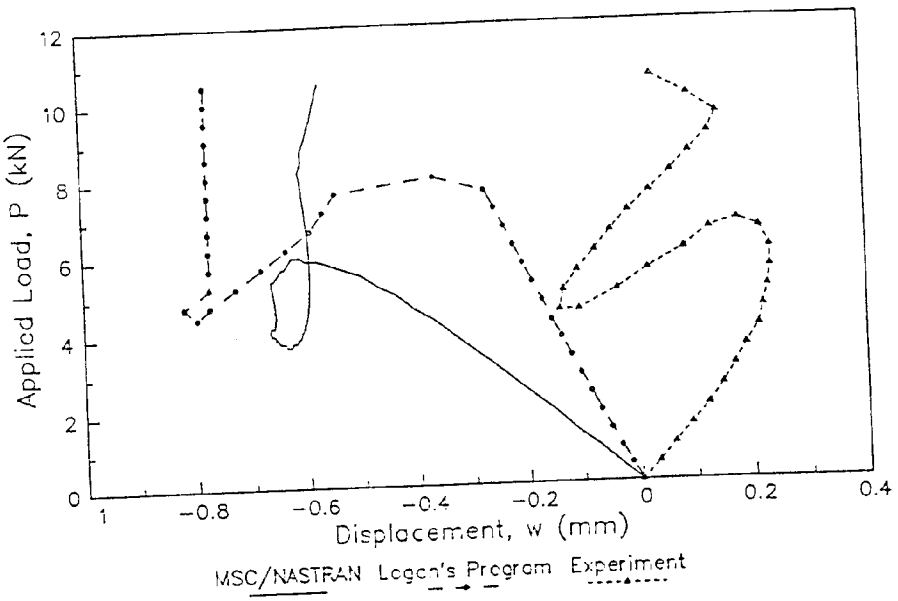

Fig. 4.5 Load Displacement Curve at Node 14

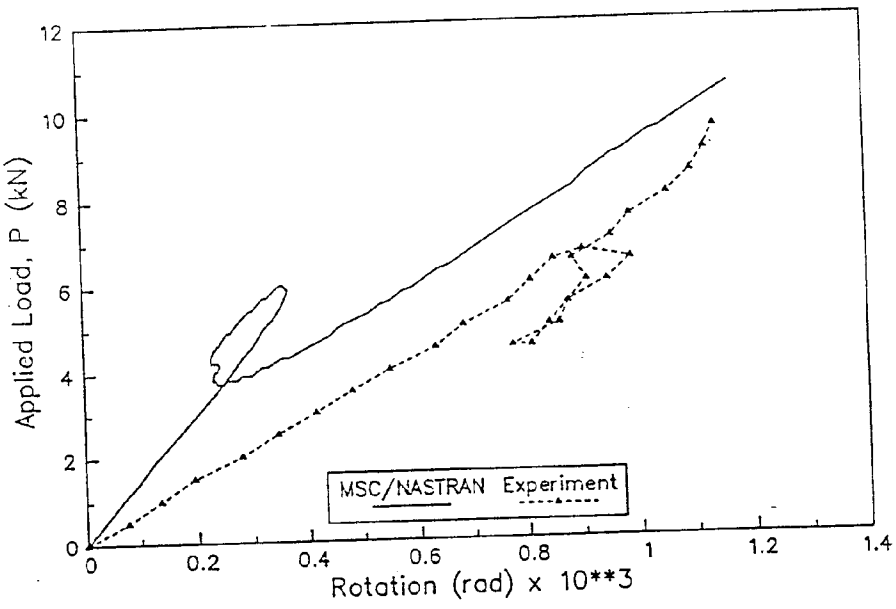

Fig. 4.6 Support Rotation at Node 58

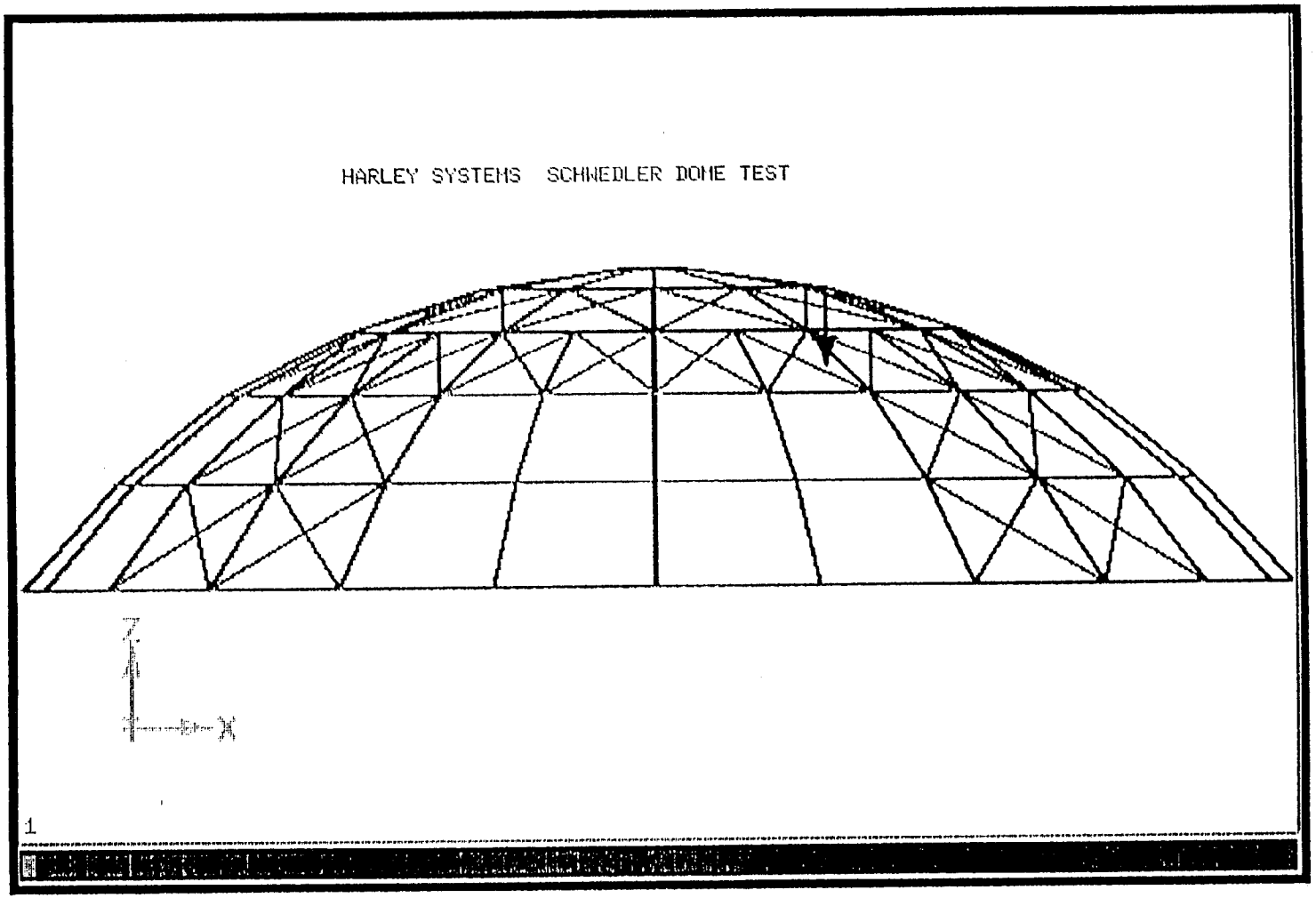

Fig. 4.7 Geometry of the Schwendler Dome

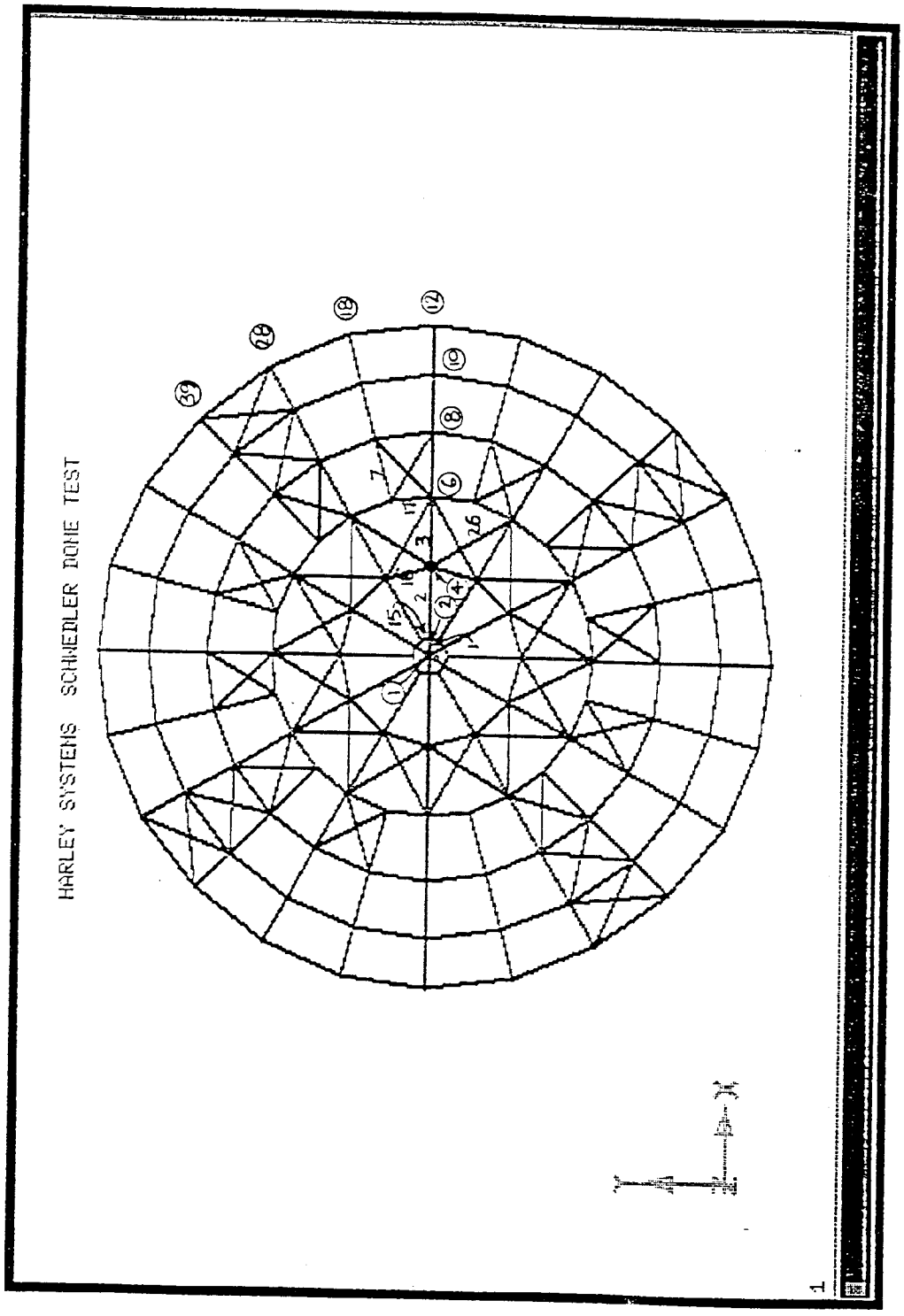

Fig. 4.8 Plan View of the Schwendler Dome

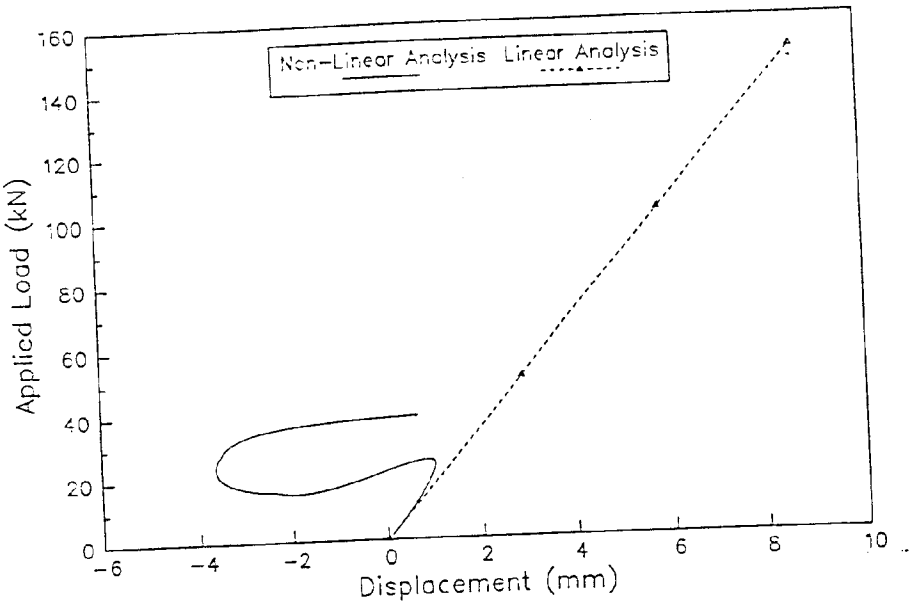

Fig. 4.9 Load Displacement Curve at Node 1

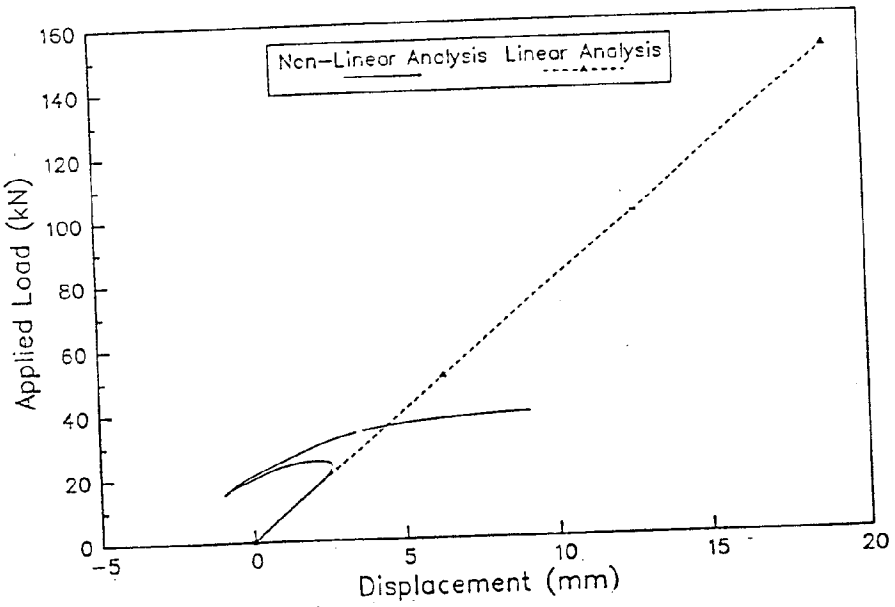

Fig. 4.10 Load Displacement Curve at Node 2

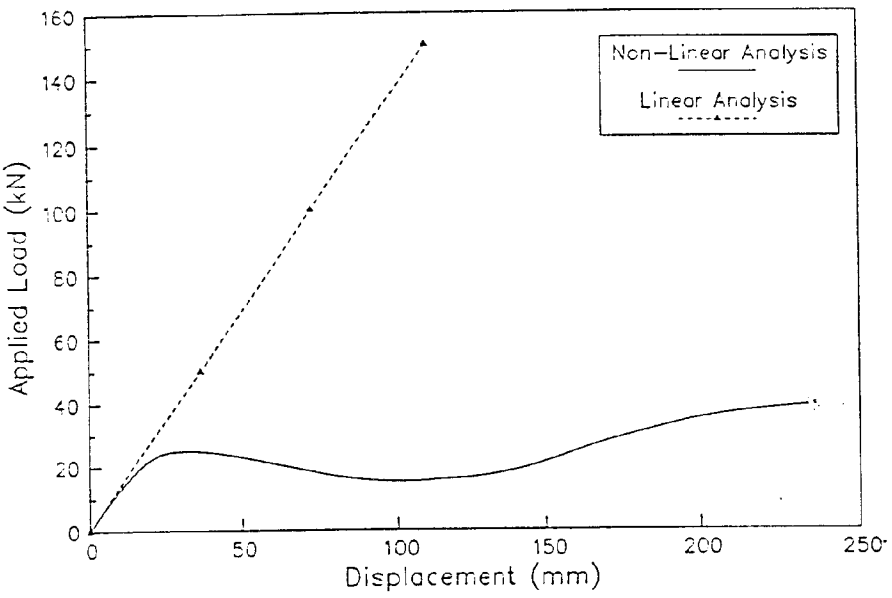

Fig. 4.11 Load Displacement Curve at Node 4

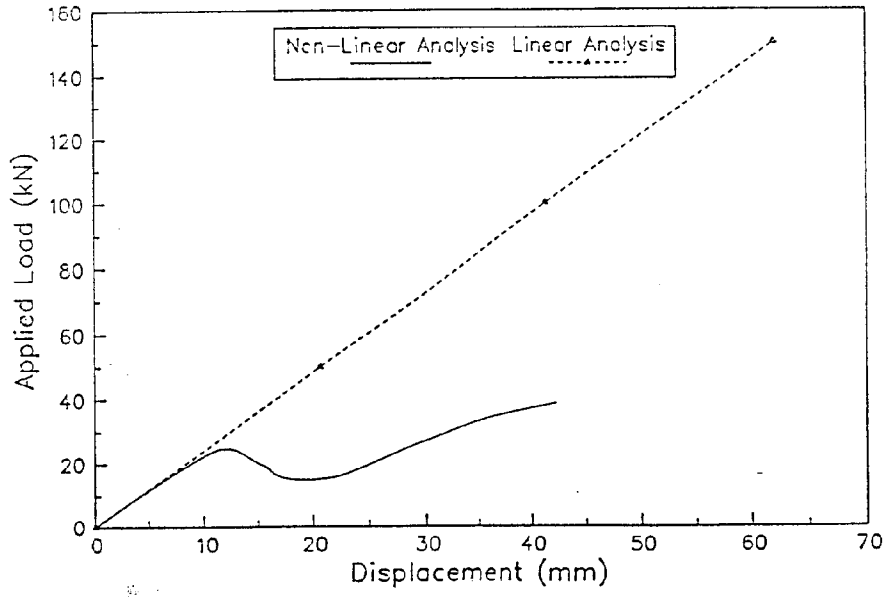

Fig. 4.12 Load Displacement Curve at Node 6

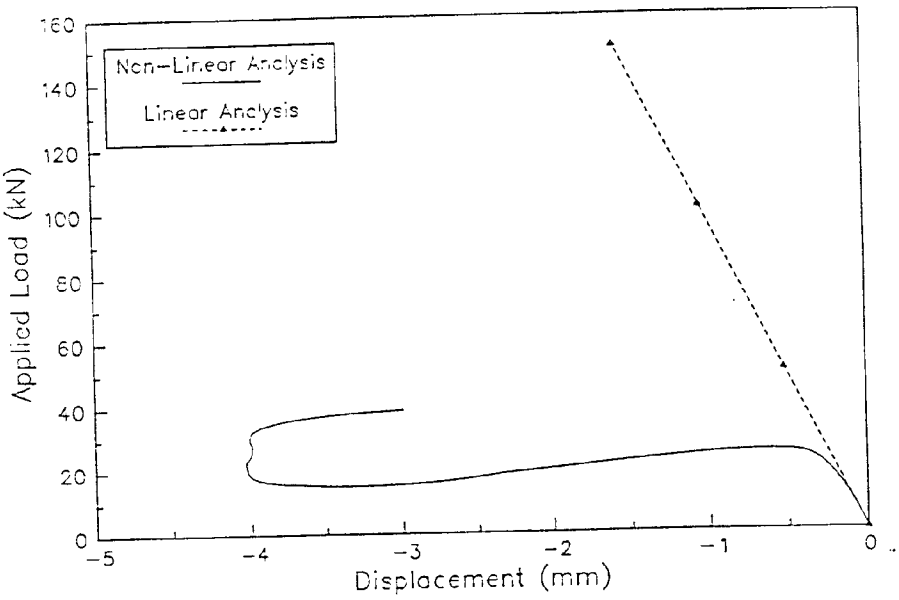

Fig. 4.13 Load Displacement Curve at Node 8

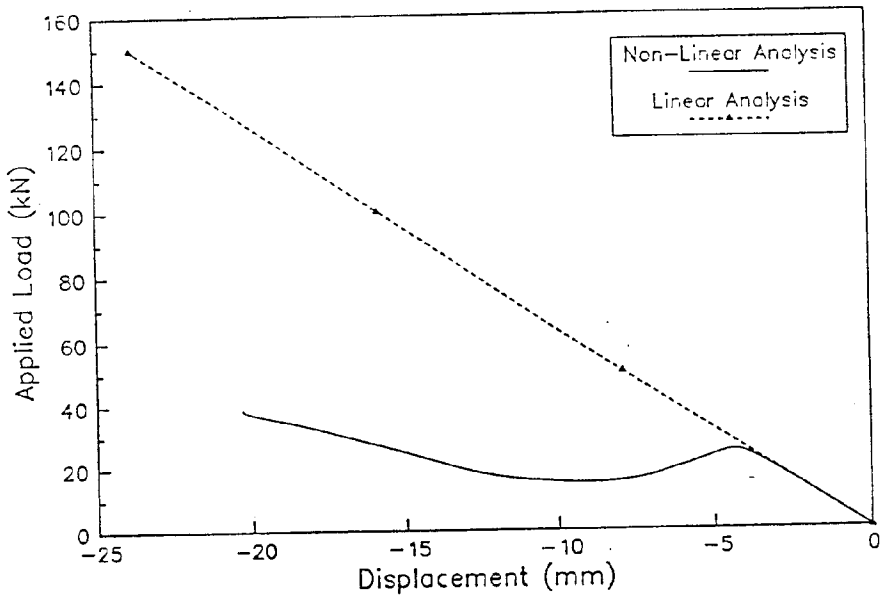

Fig. 4.14 Load Displacement Curve at Node 10

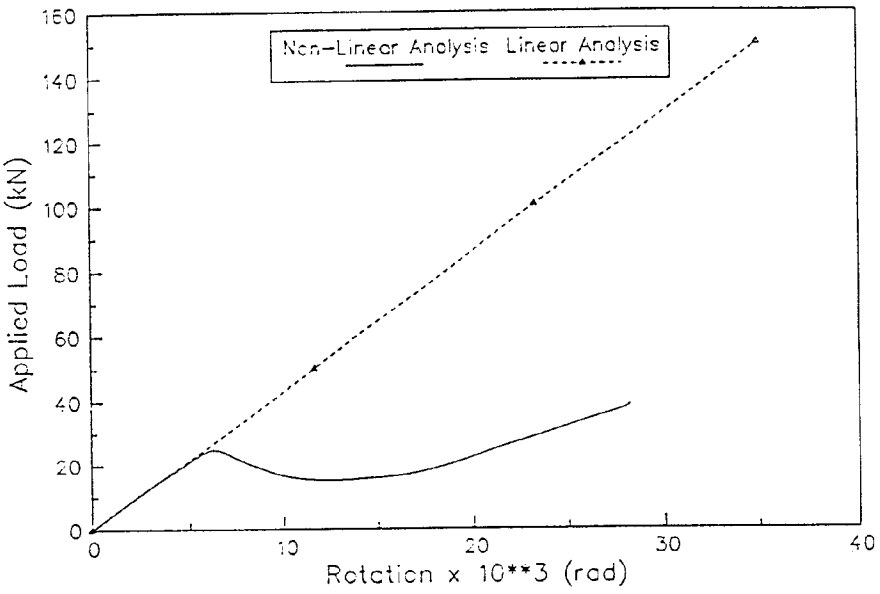

Fig. 4.15 Support Rotation at Node 12

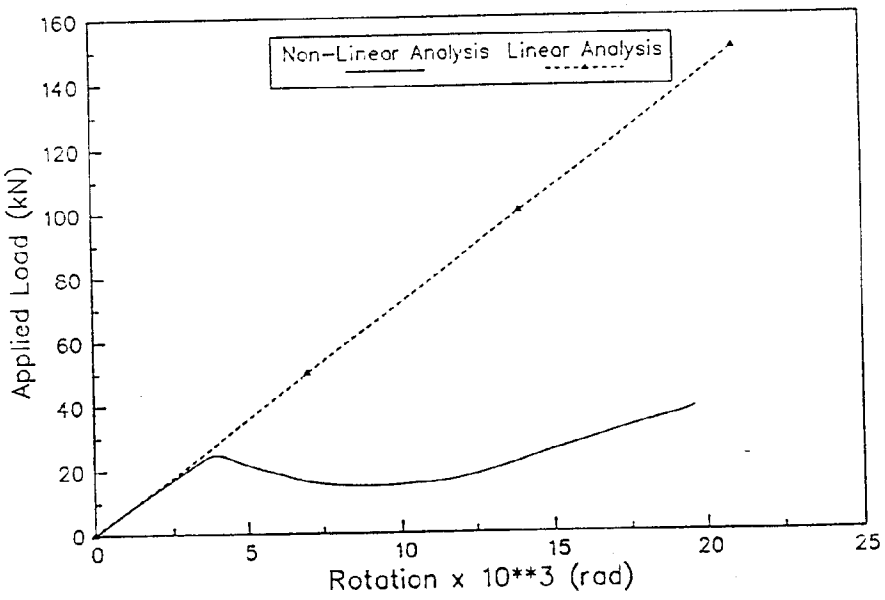

Fig. 4.16 Support Rotation at Node 18

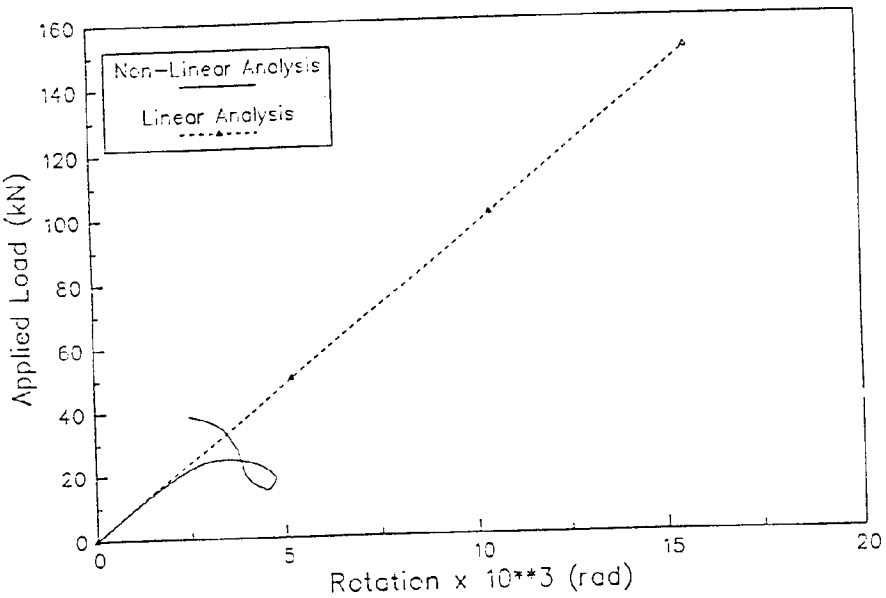

Fig. 4.17 Support Rotation at Node 28

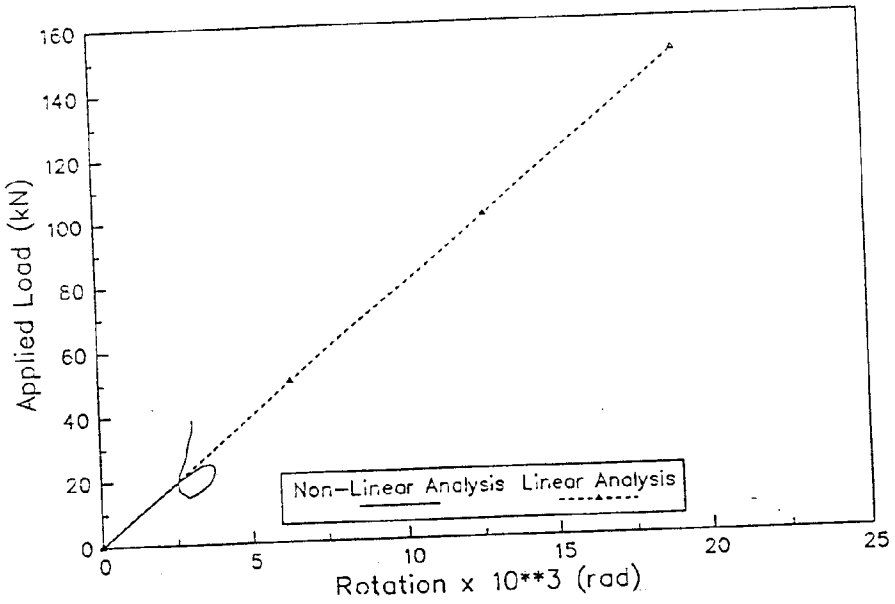

Fig. 4.18 Support Rotation at Node 39

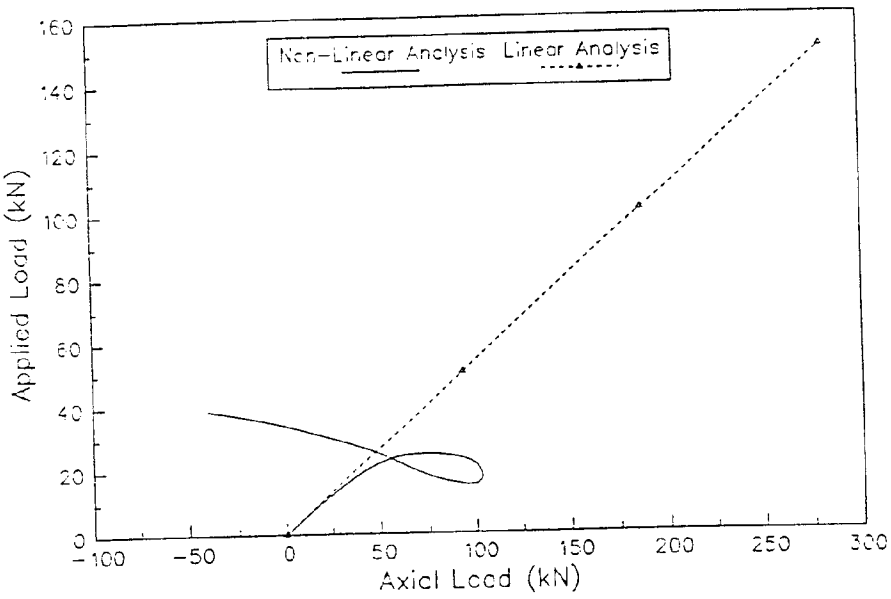

Fig. 4.19 Axial Load at Member 1

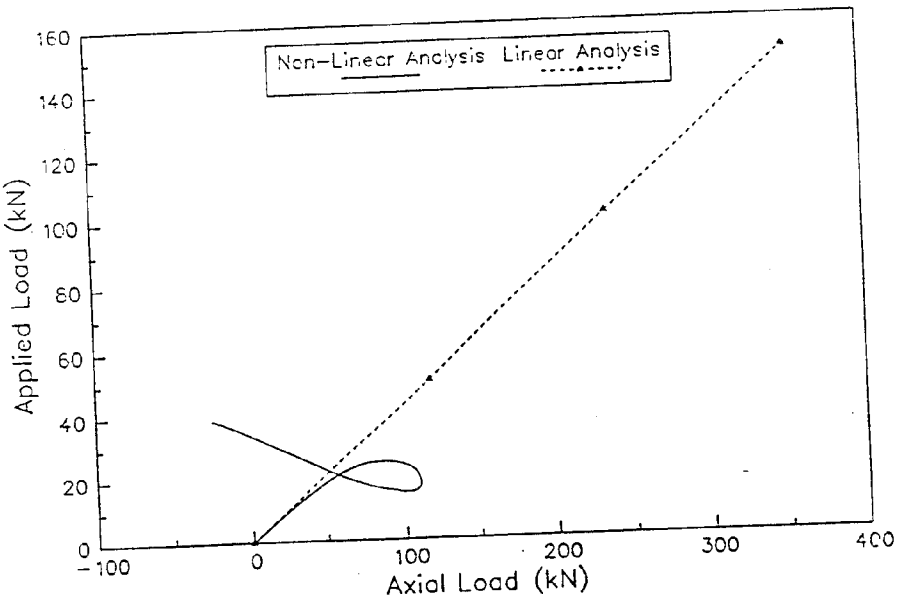

Fig. 4.20 Axial Load at Member 2

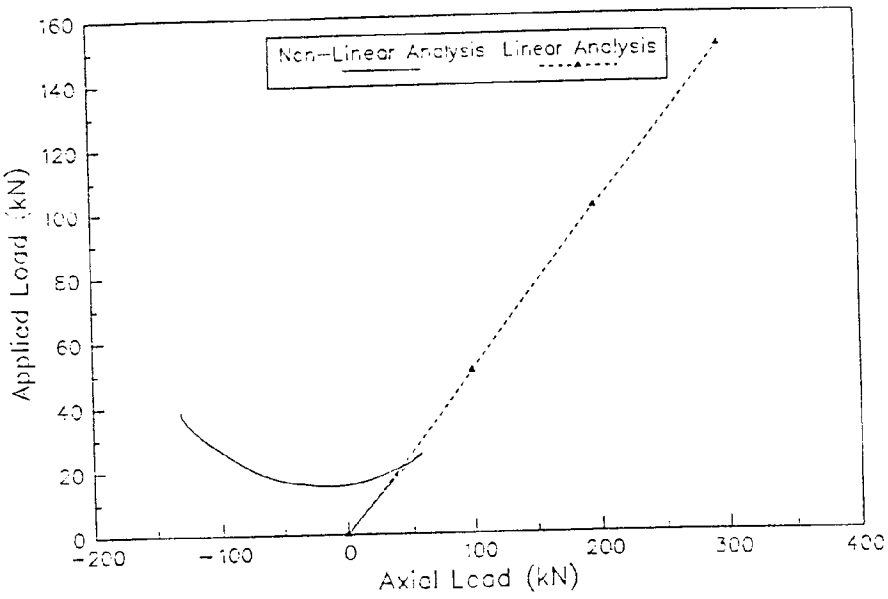

Fig. 4.21 Axial Load at Member 3

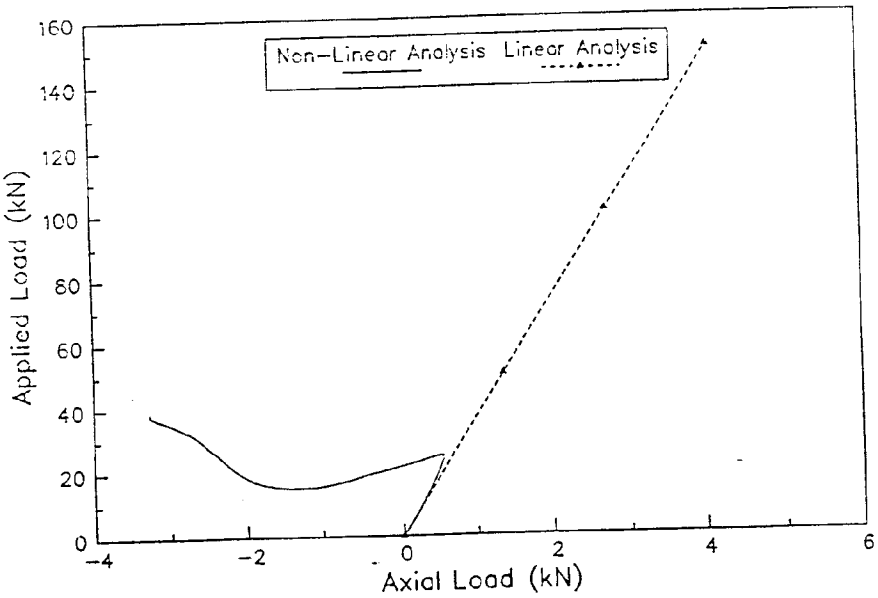

Fig. 4.22 Axial Load at Member 7

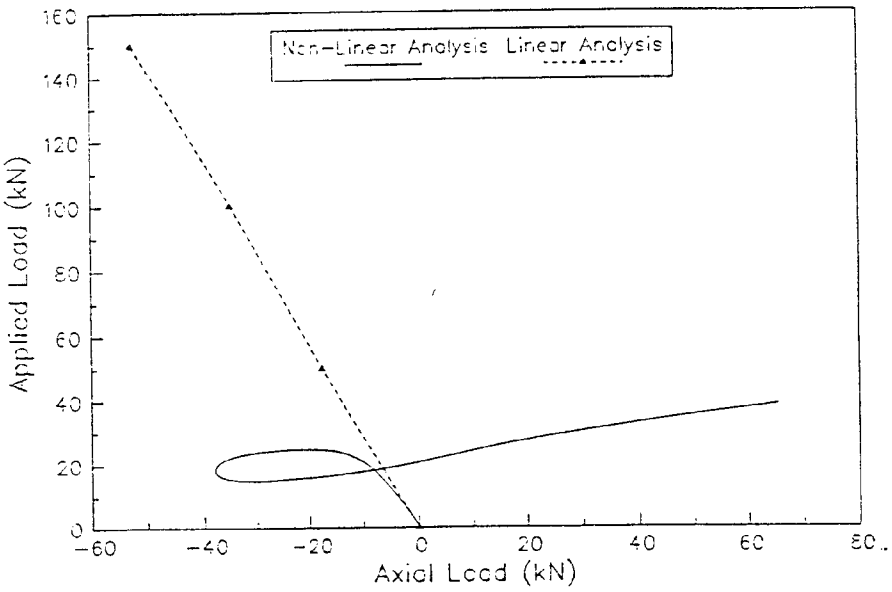

Fig. 4.23 Axial Load at Member 15

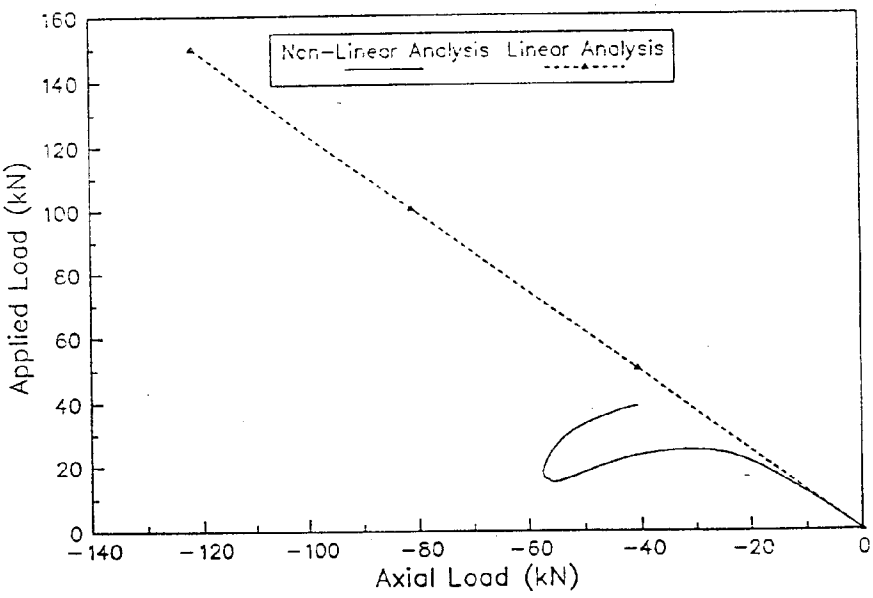

Fig. 4.24 Axial Load at Member 17

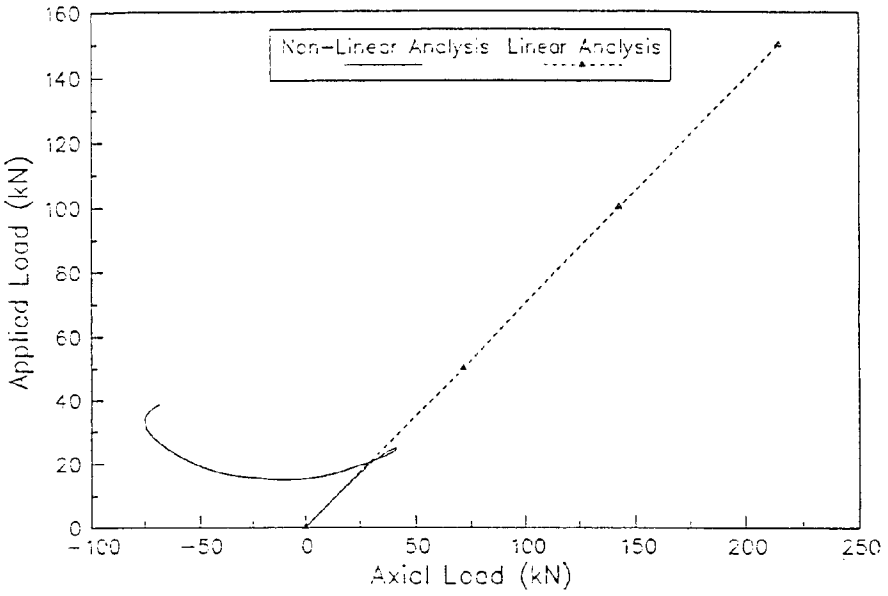

Fig. 4.25 Axial Load at Member 16

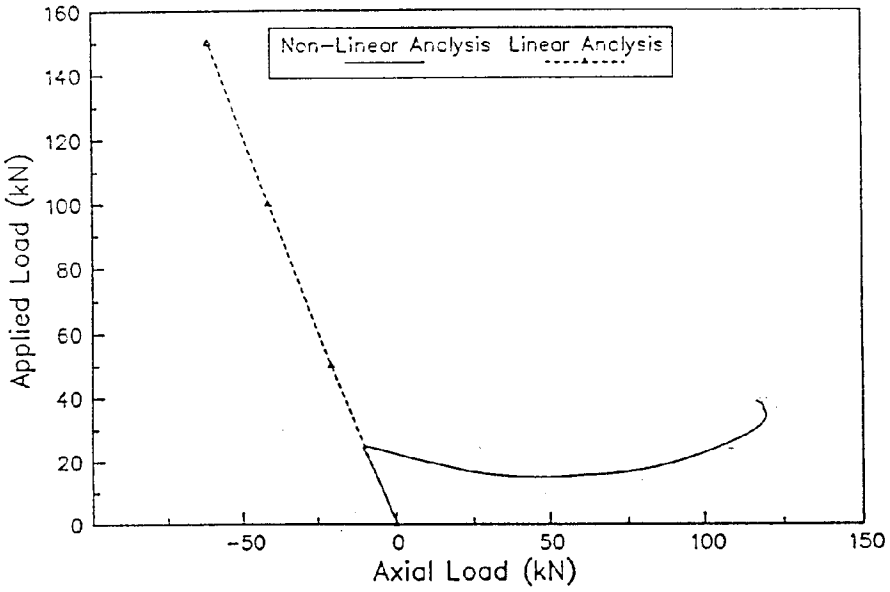

Fig. 4.26 Axial Load at Member 26